Sensors & Actuators: A. Physical 364 (2023) 114789

Contents lists available at ScienceDirect

Sensors and Actuators: A. Physical

journal homepage: www.journals.elsevier.com/sensors-and-actuators-a-physical

Laser-induced silver nanoparticles with HfO_2 shell for melamine detection

H.K. Lin [a,*], I.C. Chen [a], W.H. Lu [a], J.Y. Cheng [b], J.J. Wang [a,c]

[a] Department of Materials Engineering, National Pingtung University of Science and Technology, Pingtung, Taiwan
[b] Research Centre for Applied Sciences, Academia Sinica, Taipei, Taiwan
[c] Department of Laser Micro-processing Technology, Industrial Technology Research Institute Southern Region Campus, Tainan, Taiwan

ARTICLE INFO

Keywords:
Sputter
Laser dewetting
LSPR
Nanoparticle
Melamine

ABSTRACT

Pure Ag nanoparticles (NPs) were synthesized on glass substrates by laser dewetting and then modified with hafnium dioxide (HfO_2) by a sputtering process. The optical properties and melamine detection performance of the modified Ag NPs were investigated. The results showed that the Ag NPs produced in the laser dewetting process with accumulated unit volume energies of 0.2–3.67 kJ/mm^{3}s had a size of 51–107 nm. Furthermore, the Ag NPs exhibited an optical absorption peak in the wavelength range of 429–495 nm. A strong Raman signal fingerprint peak was observed at 701 cm^{-1} in a 10^{-3} M melamine solution. The corresponding analytical enhancement factor (AEF) was 1.9×10^2. For the Ag@HfO_2 NPs, localized surface plasmon resonance (LSPR) occurred at 584–800 nm, with an AEF of 2.3×10^4. The limit of detection for melamine using the Ag@HfO_2 NPs was 10^{-5} M. Moreover, the Ag@HfO_2 NPs showed a more stable Raman spectrum than the Ag NPs. Hence, the potential of the Ag@HfO_2 NPs for melamine detection was confirmed.

1. Introduction

Melamine (1,3,5-Trizaine-2,4,6-triamine) is a triazine nitrogen-containing heterocyclic organic compound ($C_3H_6N_6$) with a high nitrogen content, high hardness, superior heat resistance, and good flame retardancy. It is commonly used to fabricate melamine tableware, thermosetting coatings, retardant, and so on. However, following the tainted milk powder incident in China in 2008, the addition of melamine to food products has been recognized as an important concern [1]. Although melamine has low toxicity, its long-term consumption can lead to kidney stones, bladder cancer, and other diseases [2]. Therefore, accurate methods for determining the concentration of melamine in foods and beverages has become an important issue in the food safety and monitoring field.

Various methods are available for detecting melamine, including high performance liquid chromatography ultraviolet spectrometry (HPLC/UV), liquid chromatography tandem mass spectrometry (LC-MS/MS), and gas chromatography mass spectrometry (GC/MS). Two screening methods dedicated to the determination of melamine in cow's milk. Screening methods are enzyme-linked immunosorbent assay (ELISA) and liquid chromatography coupled to ultraviolet detection. ELISA offers a semi-quantitative determination of melamine and allows the rapid detection of melamine in several samples analyzed in parallel [3]. Moreover, some studies verified that the detection of melamine in aquaculture feed and milk samples based on molecularly imprinted solid-phase extraction and N-methylmesoporphyrin IX/G-quadruplex structure, respectively [4,5]. Among these methods, one of the most commonly used is Raman spectrometry, which measures the vibration spectrum of a specific molecule or lattice and is frequently combined with the detection of nanoparticles (NPs) in a technique known as surface-enhanced Raman scattering (SERS) [6,7]. Zhao [8] reported that determination of melamine by SERS spectroscopy using starch-coated silver nanoparticles as substrates. The limits of detection (LOD) of the melamine in the range of 2.0–50.0 mg L^{-1} were computed based on 3 times the standard deviation of the blank signal. Inamuddin et al. [9] showed an eco-friendly and robust silver nanoparticles (AgNPs) as a simple and sensitive probe for the detection of melamine in biological samples. The limit of detection was 0.070 ppm.

In addition, some studies showed that nanoparticles were synthesized on different substrates by a chemical process and the SERS signal intensity of melamine could be observed. Cheng [10] reported that SERS-active AgNR array substrates were fabricated using oblique angle deposition in a custom-built electron beam evaporation system. The determination of melamine content in animal feed was developed and the limits of detection were 0.9 μg·g^{-1}. The gold nanoparticles (AuNPs) onto g-C3N4/Ni3N (Au/g-C3N4/Ni3N) nanocomposite material were

* Corresponding author.
E-mail address: HKLin@mail.npust.edu.tw (H.K. Lin).

https://doi.org/10.1016/j.sna.2023.114789
Received 3 September 2023; Received in revised form 27 October 2023; Accepted 31 October 2023
Available online 3 November 2023
0924-4247/© 2023 Elsevier B.V. All rights reserved.

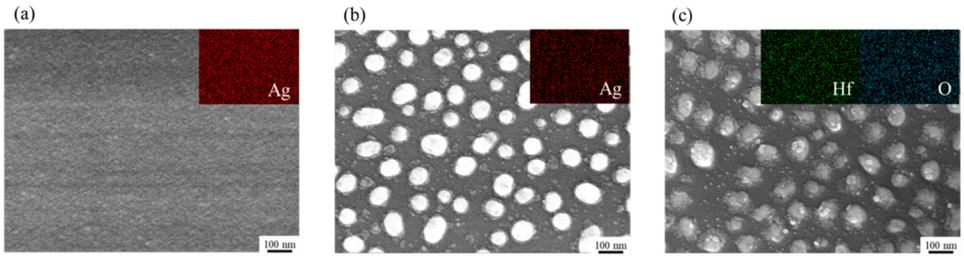

Fig. 1. SEM surface morphology images of: (a) Ag film, (b) Ag NPs, and (c) Ag@HfO_2. (Note that EDS mapping results are provided in upper-right corner in each case.).

used for the SERS-based melamine detection and the average enhancement factor is evaluated to be 2.56×10^7 [11]. Zinc gallate ($ZnGa_2O_4$) nanorod arrays grown on a Si substrate by chemical vapor deposition were used as templates to fabricate SERS substrates by deposition of Ag nanoparticles onto the $ZnGa_2O_4$ nanorod surfaces [12]. The SERS signal intensity of melamine decreased greatly as the concentration of benzoic acid was increased. A significant SERS enhancement from silver nanoparticle-decorated ZnO nanowires to the Raman spectra of melamine solutions was demonstrated [13]. In addition. hydrophobic carbon/silver (oCDs/Ag) nanoparticles were synthesized in one step by mixing hexadecylpyridinium chloride monohydrate and $AgNO_3$ in the presence of NaOH. The SERS platform was applied in the melamine detection in water and milk, which exhibits a good linear property in the range from 0.01 ppm to 100 ppm, and low limit detection of 9 ppb [14]. Yang et al. [15] also reported that detection of melamine by using carboxyl-functionalized Ag-covalent organic framework as a novel SERS substrate. The linear range was 1–20 μg/L and the limit of detection (LOD) was 0.68 μg/L in liquid milk. Raman spectroscopy provides a quick and effective means of detecting melamine and is characterized by a prominent peak at 682 cm^{-1} in the Raman spectrum, referred to as the fingerprint peak of melamine [16–24].

Among the many NPs which have been developed, Ag and Au NPs have a particularly good SERS performance due to their special optical properties, which result in a unique and strong localized surface plasmon resonance (LSPR) phenomenon [14] and the SERS detection is widely used in many applications. One of the most convenient methods for fabricating metal NPs is that of laser dewetting, in which the spontaneous self-assembly of NPs is induced through the effects of surface energy minimization in response to the irradiation of the metal layer by a laser beam [25–28]. In recent years, a new Raman spectroscopy technique known as shell-isolated nanoparticles enhanced Raman spectroscopy (SHINERS) has been proposed [15], in which an ultra-thin ceramic shell is deposited on the surface of the metal NPs to enhance the Raman signal. The ceramic shell not only maintains the spherical shape of the NPs, but also prevents their direct contact with the analyte, thereby reducing the background noise and improving the stability and reproducibility of the Raman signal. However, the choice of shell material is critically important. As a protective layer, hafnium dioxide (HfO_2) has excellent stability, reproducibility, and low thermal conductivity. Furthermore, as a shell coating, it allows light to penetrate and minimizes the impact of photoelectricity on the metal NPs [16]. Consequently, this study examines the feasibility for utilizing Ag NPs coated with ultrathin HfO_2shells to perform the Raman detection of melamine.

2. Materials and methods

Glass substrates with a thickness of 0.7 mm and transmittance of 90% at a wavelength of 550 nm were purchased from Ruilong Optoelectronics Co. Ltd., Taiwan. The substrates were cleaned sequentially in acetone, ethanol and deionized water for 20 min each time and were then dried in air. Ag and Ag@HfO_2 films were deposited on the cleaned glass substrates using a high-vacuum sputtering system (KD-SPUTTER+LL, Kao Duen Co., Ltd, Taiwan). The chamber pressure was reduced to less than 6×10^{-6} torr and high purity argon (Ar) gas was introduced into the chamber at a flow rate of 30 standard cubic centimeters per minute (sccm) to maintain a working pressure of 5×10^{-3} torr. The Ag and HfO_2 targets had purities of 99.99% and a diameter of 50.8 mm.

10-nm Ag films were deposited on the glass substrates using a working power of 60 W and a deposition time of 45 s. The Ag films were dewetted by a CW laser system (R4 HS Series, SPI) with a wavelength of 1070 nm and a spot size of 19 μm. The dewetting process was performed using duty cycles of 30%, 50% and 100%, laser powers of 15, 20, 25 and 30 W, and scanning speeds of 50, 100, 300 and 500 mm/s. A 2-nm layer of HfO_2 was then deposited on the Ag NPs using a working power of 80 W and deposition time of 43 s

The surface morphologies of the NPs were observed by a Field-Emission Scanning Electron Microscope (JSM-7600 F). The size and number of the NPs formed under the different dewetting condition were quantified using ImageJ software (National Institutes of Health, USA). The optical properties of the NPs were analyzed using a UV–vis spectrophotometer (Lambda 35, PerkinElmer) at wavelengths ranging from 300 to 800 nm. The feasibility of the Ag NPs for SERS detection, and the Ag@HfO_2 for SHINERS detection, was investigated using aqueous melamine solutions with concentrations ranging from 10^{-3}–10^{-6} M". The SERS spectra of the melamine solutions for the various Ag NP and Ag@HfO_2 substrates were acquired by a confocal Raman microspectrometer (MRI532S) with a wavelength of 532 nm, a Raman power of 30 mW, an integration time of 10 s, and 5 times.

3. Results and discussions

The as-deposited Ag film had a smooth and continuous surface, as shown in Fig. 1(a). However, in the laser dewetting process, the laser energy induced the formation of silver NPs in accordance with the principle of surface energy minimization (see Fig. 1(b)). A 2-nm HfO_2 film was deposited on the NPs to form an Ag@HfO_2 shell structure, as shown in Fig. 1(c).

Fig. 2(a)–(c) present histograms of the NP size for the Ag films dewetted using duty cycles of 100%, 50% and 30%, respectively, and laser powers and speeds in the range of 15–30 W and 50–500 mm/s. It is seen that the overall particle size ranges from 51 to 107 nm. For a given duty cycle and laser speed, the NP size decreases as the laser energy (i.e., laser power) increases. The minimum particle size of 51 nm is obtained at a duty cycle of 30%, a scanning speed of 50 mm/s, and a laser power of 30 W. For a constant duty cycle and laser power, the NP size increases with an increasing scanning speed. The maximum particle size of 107 nm is achieved using a duty cycle of 100%, a power of 15 W, and a speed of 500 mm/s.

The dewetting results obtained under different processing conditions were quantified using the following unit volume energy (UVE) measure:

$$\mathrm{UVE}\left(\frac{\mathrm{J}}{\mathrm{mm} \wedge 3}\right) = \left(\frac{\mathrm{W}}{\pi \mathrm{R} \wedge 2 * \mathrm{V} * \mathrm{Duty\ cycle}}\right) * \mathrm{overlapping\ ratio} \quad (1)$$

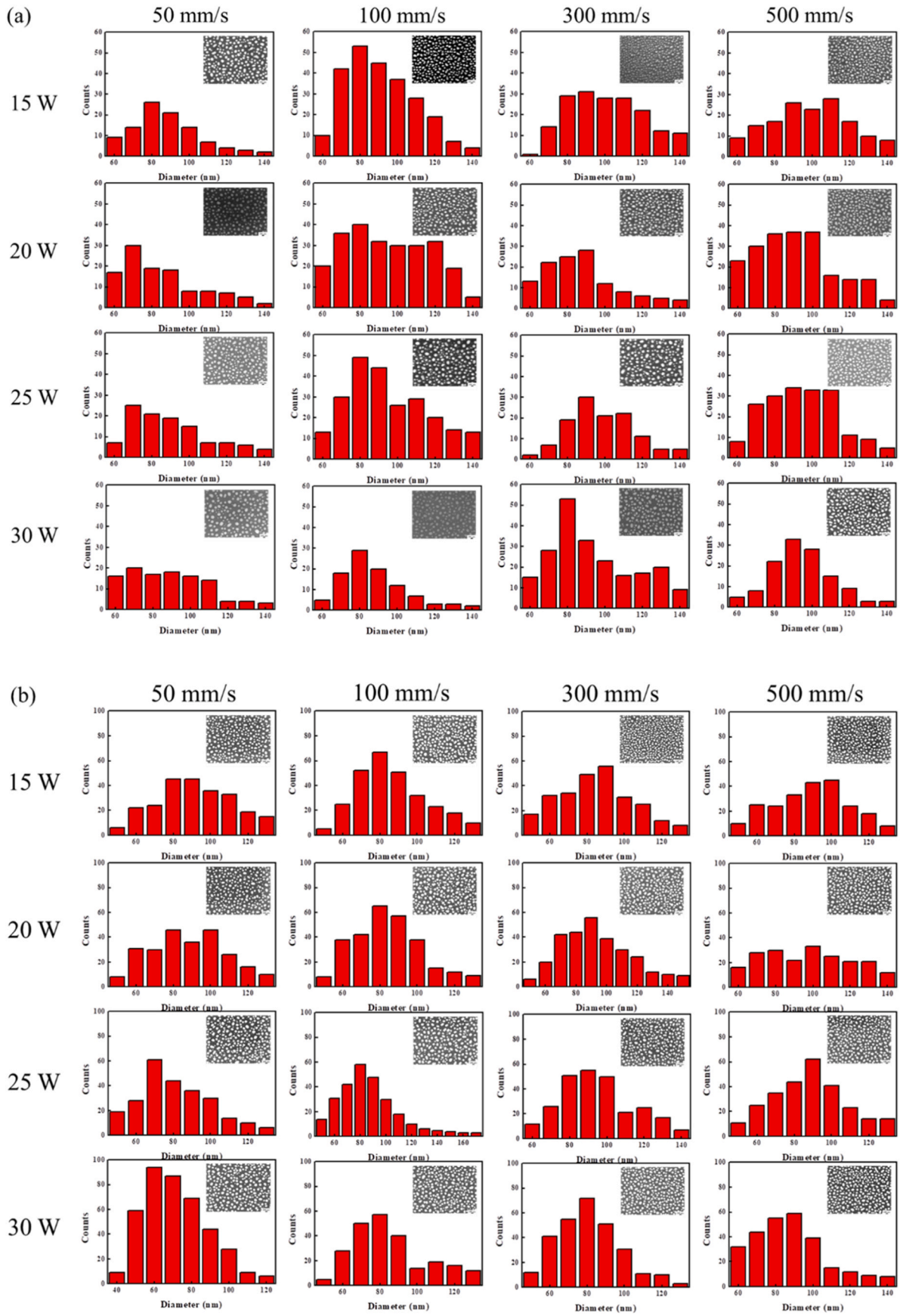

Fig. 2. Ag NP size histograms for different duty cycles, laser powers and scanning speeds: (a) 100%, (b) 50%, and (c) 30%.

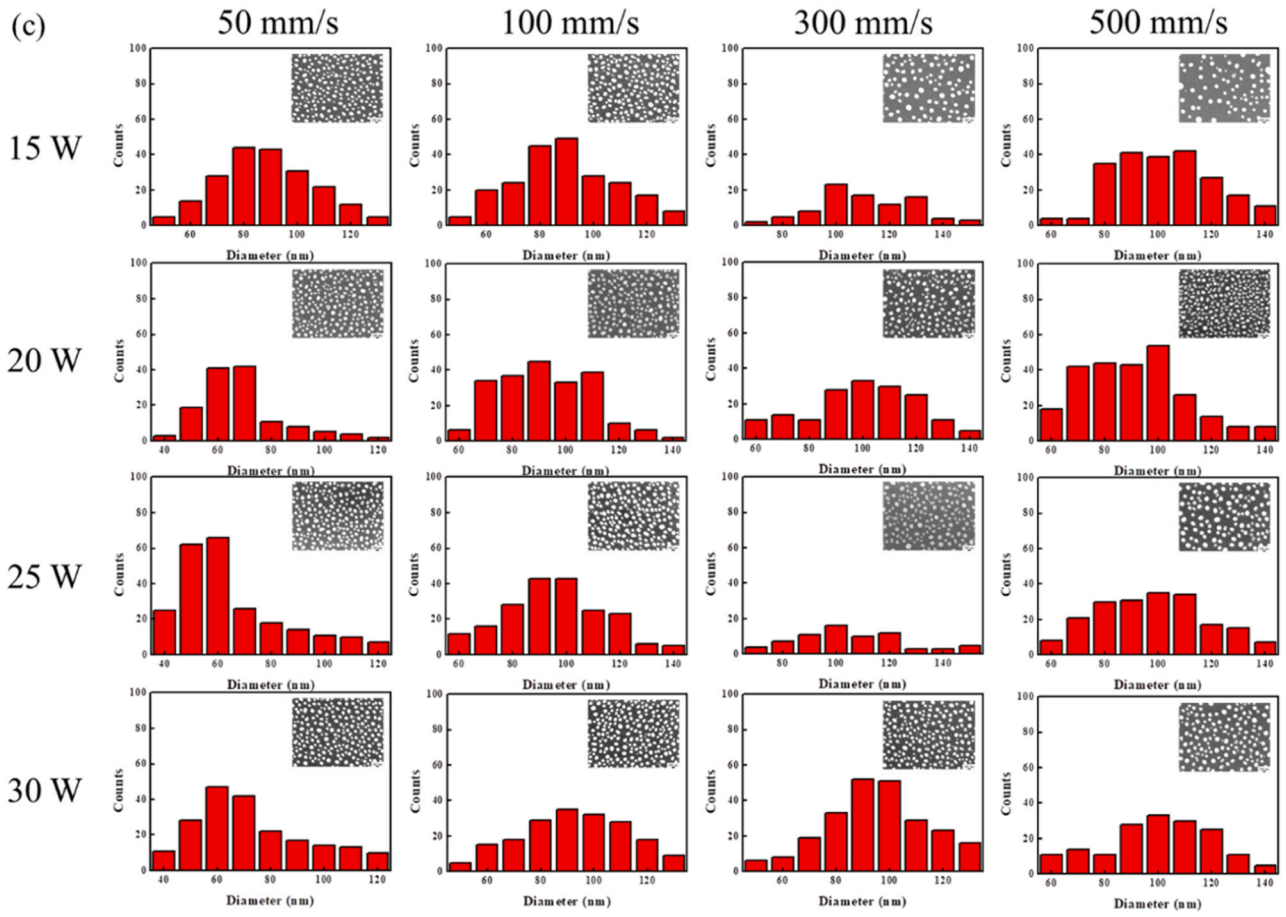

Fig. 2. (*continued*).

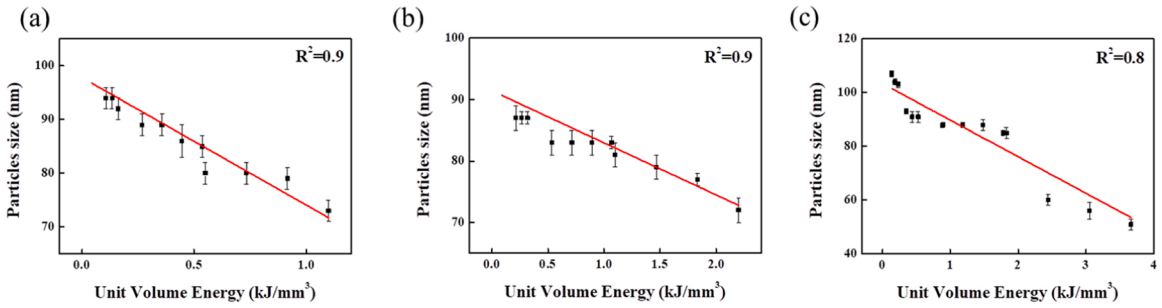

Fig. 3. Variation of Ag NP size with unit volume energy given different duty cycles: (a) 100%, (b) 50%, and (c) 30%.

where W is the laser power, R is the radius of the laser spot, V is the laser scanning speed, and the overlapping ratio is defined as

$$\text{Overlapping ratio}(\%) = \left(1 - \frac{\frac{V}{F}}{D + VT}\right) * 100\% \quad (2)$$

where F is the laser frequency, D is the diameter of the laser spot, and T is the laser pulse width (calculated as 10 μs × duty cycle).

Fig. 3 shows that the particle size reduces approximately linearly with an increasing UVE for all three duty cycle ratios. For a duty cycle of 100%, the particle size varies between 73 and 102 nm for volume energies in the range of 0.2–1.1 kJ/mm^3. For a duty cycle of 50%, the particle size varies in the range of 72–95 nm for volume energies of 0.2–2.2 kJ/mm^3. Finally, for a duty cycle of 30%, the NPs have a size of 51–107 nm for UVEs in the range of 0.2–3.67 kJ/mm^3. Overall, the results indicate that the NP size reduces with an increasing unit volume energy and a reducing duty cycle.

Fig. 4 shows the LSPR spectra of the pure Ag film, Ag NPs and Ag@HfO_2 sample, respectively. For the Ag film, no obvious absorption peak occurs. However, after the laser dewetting process, a strong absorption peak is observed at a wavelength of around 485 nm. Moreover, for the Ag@HfO_2 sample, the absorption peak shifts to 690 nm and becomes broader with a wavelength range of 584–800 nm.

Fig. 5(a–c) show the correlation between the LSPR peak spectrum of the Ag NP sample and the UVE for duty cycles of 100%, 50% and 30%, respectively. In general, the peak absorption wavelength varies in the range of 429–495 nm for the considered dewetting conditions. The absorbance peak wavelength reduces as the laser power increases due to the smaller NP size. Conversely, the wavelength peak increases with an increasing laser scanning speed due to the larger NP size. Fig. 5(d–f)

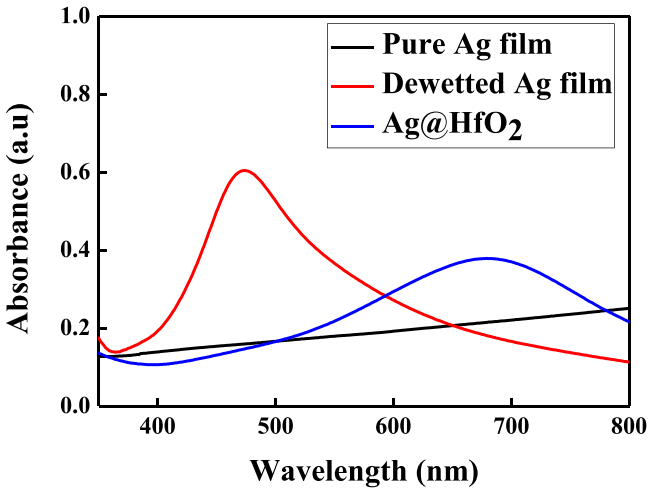

Fig. 4. LSPR spectra of pure Ag film, dewetted Ag film and Ag@HfO_2.

show the correlation between the LSPR peak position and the UVE for the Ag@HfO_2 sample. As for the Ag NP sample, the absorption wavelength decreases with an increasing UVE and a decreasing duty cycle. However, for the Ag@HfO_2 sample, the HfO_2 shell blocks the direct contact between the irradiating beam and the Ag NPs, and hence, compared to the Ag NP sample, the LSPR wavelength is increased under the same dewetting conditions.

Fig. 6(a–c) show the Raman spectra obtained for 10^{-3} M melamine solutions in contact with the Ag films processed using duty cycle ratios of 100%, 50% and 30%, respectively. The Raman signal peak of melamine has been detected during these laser parameters. For all three duty cycle ratios, the peak Raman intensity signal (i.e., the fingerprint peak of melamine) is located at around 701 cm^{-1} and is contributed by the scissor vibrations of the melamine triazine ring in the ring breathing mode II [18,23]. Fig. 6(d–f) show the Raman spectra for the Ag@HfO_2 sample in contact with the 10^{-3} M melamine solution. It is evident that the HfO_2 shell greatly increases the intensity of the Raman spectra compared to those of the uncoated Ag NP sample. The Raman peak at 493 cm^{-1} corresponds to δ (-C≡N) in-plane bending vibration of the melamine signal [19], while that at 983 cm^{-1} is produced by the mixed vibration of δ (CNC) and δ (NCN) [18], and those at 1222, 1374 and 1640 cm^{-1}, respectively, are caused by vibrations such as stretching and bending of the C-N bonds [29].

Fig. 7(a) shows the Raman spectra obtained for melamine solutions with different concentrations in contact with the Ag NP sample. The results indicate that melamine detection can be performed for concentrations of 10^{-3} to 10^{-4} M. However, the peak intensity at 701 cm^{-1} weakens as the melamine concentration reduces, and no fingerprint is observed when the concentration reaches 10^{-5} M. Fig. 7(b) shows the corresponding spectra for the Ag@HfO_2 sample. With the addition of the HfO_2 shell, melamine detection can be detected even at a weak concentration of 10^{-5} M. In other words, the HfO_2 shell increases the limit of detection (LOD) for melamine from 10^{-4} M to 10^{-5} M.

The LOD enhancement of the Ag@HfO_2 sample compared to that of the Ag NP sample can be evaluated by means of the following analytical enhancement factor (AEF):

$$AEF = (Isers/Csers)/(Irs/Crs) \quad (3)$$

where I_{sers} is the Raman intensity of the SERS-enhanced signal, C_{sers} is the melamine concentration associated with I_{sers}, I_{rs} is the intensity of the Raman signal without SERS enhancement, and C_{rs} is the melamine concentration associated with I_{rs}. Table 1 lists the LOD and AEF values of the Ag NP and Ag@HfO_2 samples. The AEF values of the two samples are 1.9×10^2 and 2.3×10^4, respectively. In other words, the HfO_2 shell structure increases the AEF by around 120 times.

To investigate the practical feasibility of the Ag@HfO_2 sample as a SHINERS substrate, the Ag NP and Ag@HfO_2 samples were held in air for up to 4 weeks. Fig. 8 shows the Raman spectra obtained for the two samples after different aging periods for a melamine solution with a concentration of 10^{-3} M. The Ag NP sample shows a clear melamine fingerprint peak at 701 cm^{-1}; however, the intensity of the peak weakens as the aging time increases, and no signal is detected after 28

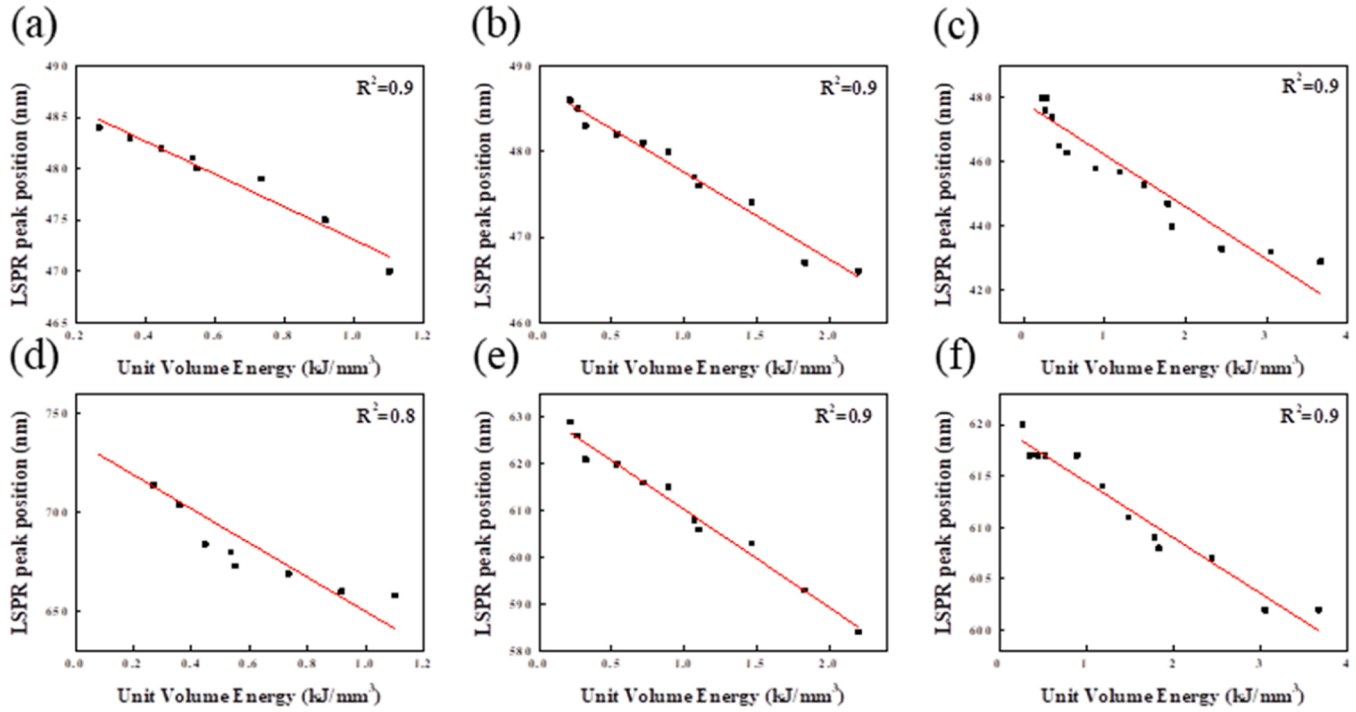

Fig. 5. Variation of LSPR peak position with unit volume energy for (a, b, c) dewetted Ag film and (d, e, f) Ag@HfO_2 for different duty cycles: (a, d) 100%, (b, e) 50%, (c, f) 30%.

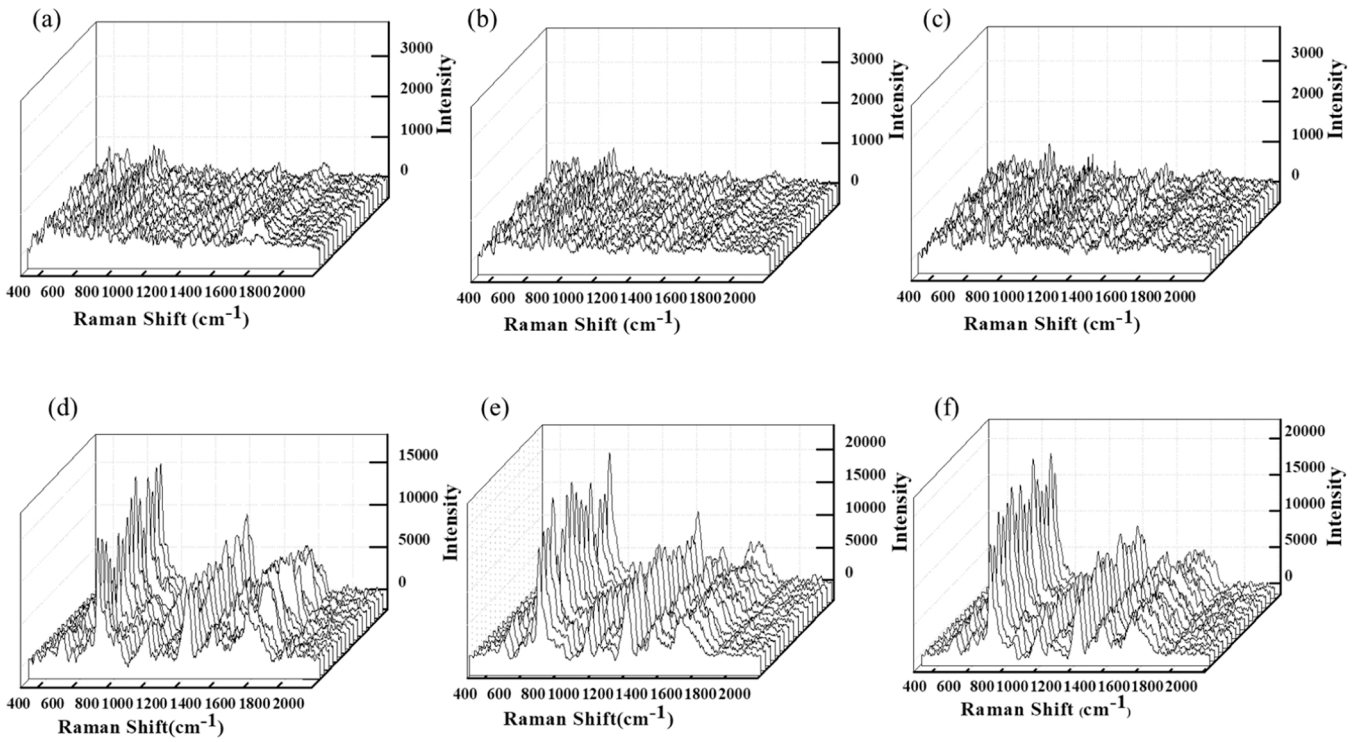

Fig. 6. Raman spectra of (a, b, c) dewetted Ag film and (d, e, f) Ag@HfO_2 for 10^{-3} M melamine for different duty cycles: (a, d) 100%, (b, e) 50%, and (c, f) 30%.

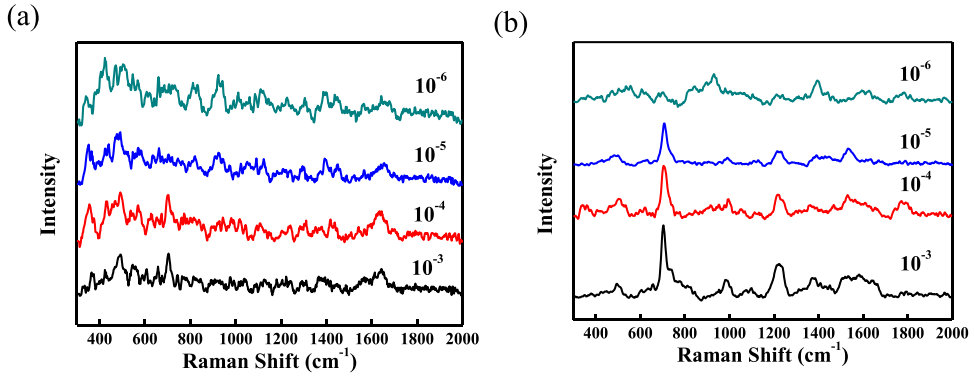

Fig. 7. LOD for different melamine concentrations using: (a) Ag NPs and (b) Ag@HfO_2.

Table 1
LOD and AEF of Ag NPs and Ag@HfO_2.

Sample	LOD (M)	AEF
Ag NPs	10^{-4}	1.9×10^2
Ag@HfO_2	10^{-5}	2.3×10^4

days (Fig. 8(a)). By contrast, the Ag@HfO_2 sample provides an obvious and strong melamine peak even after 28 days (Fig. 8(b)). Moreover, the Ag@HfO_2 sample provides a stable Raman response over the complete aging period, as shown in Fig. 8(c). In other words, the Ag@HfO_2 sample provides a feasible, long-term SHINERS substrate for melamine detection.

4. Conclusions

This study has used a laser dewetting process to produce Ag NPs on glass substrates. The NPs have been coated with HfO_2 and applied for melamine detection. The results have shown that, in the dewetting process, Ag NPs are formed for unit volume energy values in the range of 0.2–3.67 kJ/mm^3. The Ag NPs have a regular array and uniform size with a mean diameter of around 51–107 nm, depending on the processing conditions. The LSPR absorbance wavelength of the Ag NP sample varies in the range of 429–495 nm and undergoes a red shift as the unit volume energy decreases. For the Ag@HfO_2 sample, the LSPR absorbance wavelength lies in the range of 584–800 nm. When applied to melamine detection, the Ag NP sample has shown a Raman limit of detection of 10^{-4} M melamine and an AEF of 1.9×10^2. However, the Ag@HfO_2 sample has shown a more stable fingerprint peak, a lower detection limit of 10^{-5} M, and an increased AEF of 2.3×10^4. Hence, the potential of the Ag@HfO_2 sample for melamine detection has been confirmed.

CRediT authorship contribution statement

H.K. Lin: writing, review and funding acquisition. **I.C. Chen:** data collection, methodology, and visualization. **W.H. Lu:** investigation and formal analysis. **J.Y. Cheng:** review and supervision. **J.J. Wang:**

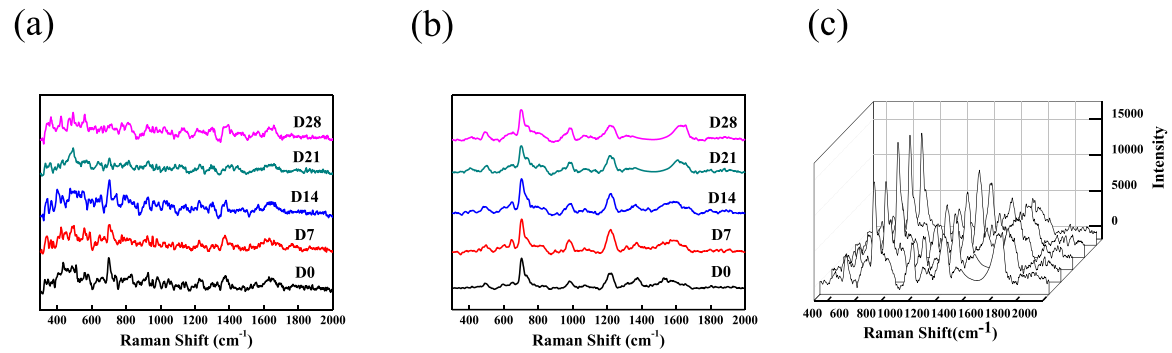

Fig. 8. Raman spectra of 10^{-3} M melamine after different holding times: (a) Ag NPs, (b) Ag@HfO_2 and (c) Ag@HfO_2 after 28 days.

investigation, and original draft preparation.

Declaration of Competing Interest

The authors declare that they have no known competing financial interests or personal relationships that could have appeared to influence the work reported in this paper.

Data availability

Data will be made available on request.

Acknowledgments

The authors gratefully acknowledge the financial support provided to this study by National Science and Technology Council, ROC, under Project No. NSTC 112-2637-E-020-004.

References

[1] Y.C. Tyan, M.H. Yang, S.B. Jong, C.K. Wang, J. Shiea, Melamine contamination, Anal. Bioanal. Chem. 395 (3) (2009) 729–735.
[2] C.G. Skinner, J.D. Thomas, J.D. Osterloh, Melamine toxicity, J. Med Toxicol. 6 (1) (2010) 50–55.
[3] P. Lutter, M.-C. Savoy-Perroud, E. Campos-Gimenez, L. Meyer, T. Goldmann, M.-C. Bertholet, P. Mottier, A. Desmarchelier, F. Monard, C. Perrin, F. Robert, T. Delatour, Screening and confirmatory methods for the determination of melamine in cow's milk and milk-based powdered infant formula: validation and proficiency-tests of ELISA, HPLC-UV, GC-MS and LC-MS/MS, Food Control 22 (6) (2011) 903–913.
[4] J. Wang, Y. Wu, Q. Wu, L. Li, Y. Wang, H. Yang, Highly sensitive detection of melamine in milk samples based on N-methylmesoporphyrin IX/G-quadruplex structure, Microchem. J. 155 (2020), 104751.
[5] Ziru Lian, Zhenlin Liang, J. Wang, Determination of melamine in aquaculture feed samples based on molecularly imprinted solid-phase extraction, J. Sep. Sci. 38 (2015) 3655–3659.
[6] M. Fleischmann, P.J. Hendra, A.J. McQuillan, Raman spectra of pyridine adsorbed at a silver electrode, Chem. Phys. Lett. 26 (2) (1974) 163–166.
[7] D. Graham, The next generation of advanced spectroscopy: surface enhanced Raman scattering from metal nanoparticles, Angew. Chem. Int Ed. Engl. 49 (49) (2010) 9325–9327.
[8] Y. Zhao, Y. Tian, P. Ma, A. Yu, H. Zhang, Y. Chen, Determination of melamine and malachite green by surface-enhanced Raman scattering spectroscopy using starch-coated silver nanoparticles as substrates, Anal. Methods 7 (19) (2015) 8116–8122.
[9] S.Kanchi Inamuddin, One-pot biosynthesis of silver nanoparticle using Colocasia esculenta extract: colorimetric detection of melamine in biological samples, J. Photochem. Photobiol. A 391 (2020), 112310.
[10] J. Cheng, X.O. Su, Y. Yao, C. Han, S. Wang, Y. Zhao, Highly sensitive detection of melamine using a one-step sample treatment combined with a portable Ag nanostructure array SERS sensor, PLoS One 11 (4) (2016), e0154402.
[11] M. Tiwari, A. Singh, D. Thakur, S.K. Pattanayek, Graphitic carbon nitride-based concoction for detection of melamine and R6G using surface-enhanced Raman scattering, Carbon 197 (2022) 311–323.
[12] L. Chen, D. Jiang, X. Liu, G. Qiu, $ZnGa_2O_4$ Nanorod arrays decorated with Ag nanoparticles as surface-enhanced Raman-scattering substrates for melamine detection, ChemPhysChem 15 (8) (2014) 1624–1631.
[13] A.L. Cook, C.S. Carson, C.E. Marvinney, T.D. Giorgio, R.R. Mu, Sensing trace levels of molecular species in solution via zinc oxide nanoprobe Raman spectroscopy, Res. Article 48 (8) (2017) 1116–1121.
[14] J. Qiu, Y. Chu, Q. He, Y. Han, Y. Zhang, L. Han, A self-assembly hydrophobic oCDs/Ag nanoparticles SERS sensor for ultrasensitive melamine detection in milk, Food Chem. 402 (2023), 134241.
[15] Z. Yang, C. Ma, J. Gu, Y. Wu, C. Zhu, L. Li, H. Gao, W. Yin, Z. Wang, G. Chen, Detection of melamine by using carboxyl-functionalized Ag-COF as a novel SERS substrate, Food Chem. 401 (2023), 134078.
[16] T.H. Chang, Y.C. Chang, C.M. Chen, K.W. Chuang, C.M. Chou, A facile method to directly deposit the large-scale Ag nanoparticles on a silicon substrate for sensitive, uniform, reproducible and stable SERS substrate, J. Alloy. Compd. 782 (2019) 887–892.
[17] K. Ge, Y. Hu, Y. Zheng, P. Jiang, G. Li, Aptamer/derivatization-based surface-enhanced Raman scattering membrane assembly for selective analysis of melamine and formaldehyde in migration of melamine kitchenware, Talanta 235 (2021), 122743.
[18] M. Tiwari, A. Singh, S. Dureja, S. Basu, S.K. Pattanayek, Au nanoparticles decorated ZnO/ZnFe(2)O(4) composite SERS-active substrate for melamine detection, Talanta 236 (2022), 122819.
[19] B. Nie, Y. Luo, J. Shi, L. Gao, G. Duan, Bowl-like Pore array made of hollow Au/Ag alloy nanoparticles for SERS detection of melamine in solid milk powder, Sens. Actuators B 301 (2019), 178087.
[20] C. Huang, S. Jiang, F. Kou, M. Guo, S. Li, G. Yu, B. Zheng, F. Xie, C. Zhang, H. Yu, J. Wang, Development of jellyfish-like ZnO@Ag substrate for sensitive SERS detection of melamine in milk, Appl. Surf. Sci. 600 (2022), 154153.
[21] G. Xiao, L. Li, A. Yan, X. He, Direct detection of melamine in infant formula milk powder solution based on SERS effect of silver film over nanospheres, Spectrochim. Acta A Mol. Biomol. Spectrosc. 223 (2019), 117269.
[22] C. Zhang, T. You, N. Yang, Y. Gao, L. Jiang, P. Yin, Hydrophobic paper-based SERS platform for direct-droplet quantitative determination of melamine, Food Chem. 287 (2019) 363–368.
[23] R. Li, J. Yang, J. Han, J. Liu, M. Huang, Quantitative determination of melamine in milk using Ag nanoparticle monolayer film as SERS substrate, Physica E 88 (2017) 164–168.
[24] H.K. Lin, T.Y. Li, I.C. Chen, Y.C. Lo, Laser-induced surface plasmon resonance and SERS performance of AgCuAl medium entropy alloy films, Mater. Lett. 333 (2023), 133701.
[25] J.J. Wang, H.K. Lin, W.S. Chuang, C.Y. Chuang, Y.H. Lin, J.C. Huang, Y.H. Lin, Laser dewetting mechanism and antibacterial properties of Cu-Al based medium entropy alloy films, J. Alloy. Compd. 903 (2022), 163893.
[26] H.K. Lin, Y.C. Chen, J.R. Lee, W.H. Lu, Y.J. Chang, Surface resonance properties of thin silver films with nanoparticles induced by pulsed-laser interference dewetting process, Int. J. Adv. Manuf. Technol. 120 (1–2) (2022) 377–384.
[27] H.K. Lin, J.J. Wang, W.H. Lu, W.S. Chuang, C.Y. Chen, H.S. Chou, J.C. Huang, Microstructure and optical properties of AgCuAl medium entropy films with nanoparticles induced by pulsed-laser dewetting, Surf. Coat. Technol. 421 (2021), 127427.
[28] H.K. Lin, C.W. Huang, Y.H. Lin, W.S. Chuang, J.C. Huang, Effects of accumulated energy on nanoparticle formation in pulsed-laser dewetting of AgCu thin films, Nanoscale Res. Lett. 16 (1) (2021) 110.
[29] N.S. Chong, K.A. Smith, S. Setti, B.G. Ooi, Application of gold and silver colloidal nanoparticles for the surface-enhanced Raman spectrometric analysis of melamine and 4-aminobiphenyl, Int. J. Environ. Technol. Manag. 16 (1–2) (2012) 3–20.

H.K. Lin received his PhD degree from National Sun Yat-sen University, Taiwan. He was an exchange scholar at University of Southern California in 2003, University of Southampton in 2017 and Bournemouth University in 2023. He is a professor at Department of Materials Engineering, National Pingtung University of Science and Technology. His research background is in areas of thin films, nanoparticle and laser.

I.C. Chen is a master student at the National Pingtung University of Science and Technology. His research background is in areas of thin films, nanoparticle and laser.

W.H. Lu received his PhD degree from National Sun Yat-sen University. He is a professor at Department of Materials Engineering and is a dean of academic affairs at National Pingtung University of Science and Technology. His research background is in areas of polymer, thin films and package.

J.Y. Cheng received his PhD degree from National Taiwan University. He is a Research Fellow since 2013 and acts as a deputy director at Research center for applied Sciences, Academia Sinica, Taiwan since 2023. His research background is in areas of cell-based micro analysis, microarray technologies and laser micromachining.

J.J. Wang received his master degree from National Pingtung University of Science and Technology in 2021. He works in Industrial Technology Research Institute now. His research background is in areas of thin films, biomaterials and laser.